Millennial and orbital-scale variability in a 54,000-year record of total air content from the South Pole ice core.

Jenna A. Epifanio[1], Edward J. Brook[1], Christo Buizert[1], Erin C. Pettit[1], Jon S. Edwards[1], John M. Fegyveresi[2], Todd A. Sowers[3], Jeffrey P. Severinghaus[4], Emma C. Kahle[5]

[1]College of Earth, Ocean, and Atmospheric Science, Oregon State University, Corvallis, 97331, USA
[2]School of Earth and Sustainability, Northern Arizona University, Flagstaff, 86011, USA
[3]The Earth and Environmental Systems Institute, Pennsylvania State University, University Park, PA, USA
[4]Scripps Institution of Oceanography, University of California San Diego, La Jolla, CA, USA
[5]Department of Earth and Space Sciences, University of Washington, Seattle, WA, USA

Correspondence to: Jenna A. Epifanio (jenna.epifanio@gmail.com)

Abstract. The total air content (TAC) of polar ice cores has long been considered a potential proxy for past ice sheet elevation. Recent work, however, has shown that a variety of other factors also influence this parameter. In this paper we present a high-resolution TAC record from the South Pole (SPC14) ice core covering the last 54,000 years and discuss the implications of the data for interpreting TAC from ice cores. The SPC14 TAC record shows multiple features of interest, including (1) long-term orbital-scale variability, (2) millennial-scale variability in the Holocene and last glacial period, and (3) a period of stability from 35 ka to 25 ka. The longer, orbital-scale variations in TAC are highly correlated with integrated summer insolation (ISI), corroborating the potential of TAC to provide an independent dating tool via orbital tuning. Large millennial-scale variability in TAC during the last glacial period is positively correlated with past accumulation rate reconstructions as well as the $\delta^{15}N\text{-}N_2$, a firn thickness proxy. These TAC variations are too large to be controlled by direct effects of temperature and too rapid to be tied to elevation changes. We propose that grain size metamorphism near the firn surface explains these changes. We note, however, that at sites with different climate histories than the South Pole, TAC variations may be dominated by other processes. Our observations of millennial-scale variations in TAC show a different relationship with accumulation rate than observed at sites in Greenland.

1 Introduction

Total air content (TAC), the total quantity of air trapped in polar ice, has long been explored as a proxy for many past climate and paleo-environmental conditions. Air pressure, temperature, and pore volume at bubble close-off control TAC in polar ice cores, as described by the ideal gas law (Martinerie et al., 1992). Variations in

TAC can reflect changes in any of these parameters. Early work in polar ice cores focused on using TAC to reconstruct ice sheet elevation changes given the dependence of atmospheric pressure on altitude (Raynaud and Lorius, 1973, Raynaud and Lebel, 1979). If elevation could be cleanly extracted from TAC records this would provide an invaluable constraint on ice sheet models, informing our understanding of ice sheet dynamics and sea

35   level change. However, while atmospheric pressure must influence TAC, the amount of air trapped in polar ice is also controlled by the pore volume at close-off, which has a complex relationship with local meteorological conditions as well as firn densification, making TAC a particularly complicated proxy (Eicher et al., 2016, Gregory et al., 2014).

The pore volume at close-off is primarily controlled by firn densification processes and is not easily

40   predicted. Previous studies have shown that variations in pore volume at bubble close-off appear to dwarf the influence of atmospheric surface pressure variations (Schwander et al., 1989, Eicher et al., 2016, Martiniere et al., 1994, Raynaud and Lebel, 1979, Krinner et al.,2000). For temperature, Raynaud and Lebel (1979) first introduced a spatial correlation between site temperature and pore volume at close-off. This was later refined by Martiniere et al. (1992) using data from late Holocene ice core samples. This effect of temperature on pore volume can be

45   empirically predicted and counteracts the effect of the local temperature from the ideal gas law. The two temperature effects on TAC have been shown to nearly cancel each other (Raynaud et al., 2007).

Previous research also showed that TAC is significantly impacted by local solar insolation on orbital time scales (Raynaud et al., 2007, Eicher et al., 2016). The proposed mechanism for this relationship requires that higher local summer insolation increases the size of snow grains in the first few meters of firn, which then

50   decreases the pore volume in these same layers as they reach bubble close-off (Raynaud et al., 1997, Arnaud, 2000). Studies at low accumulation rate polar sites have confirmed that larger firn grain sizes decrease the porosity at bubble close-off (Gregory et al, 2014, Courville et al., 2007). The relationship between TAC and local solar insolation on orbital time scales raises the possibility of directly dating TAC records using orbital tuning (Raynaud et al., 1997, Bazin et al., 2013).

55   On shorter millennial timescales, in Greenland ice core records, Eicher et al. (2016) proposed that changes in overburden pressure of the overlying firn column, driven by changes in accumulation rate, drive an inverse relationship between pore volume at close-off and accumulation rate. This process is thought to increase in importance with increasing temperature, rivalling the direct impact of changes in temperature. Eicher et al., (2016) suggest that the accumulation rate effect on TAC may be responsible for the small millennial-scale TAC

60   variations observed in Greenland ice cores. The observation is at odds with research in the low-accumulation rate Megadunes region of Antarctica, which seems to indicate that accumulation rate and pore volume at close-off are

positively correlated due to larger grain sizes in the firn at ultra-low accumulation rate sites (Gregory et al., 2014, Courville et al., 2007). However, the near-zero accumulation rate at Megadunes allows for extraordinary firn metamorphism (over hundreds of years) with the consequent reduction of pore volume, which is not comparable to Greenland.

Because previous work shows that TAC varies on multiple time scales, high-resolution data are important for fully interpreting the TAC records. To this end, we made high-resolution measurements of TAC in the South Pole ice core (SPC14). These measurements were made using a wet-extraction technique coupled with a vacuum line system that is coupled to a gas chromatograph that also provides the atmospheric methane (CH_4) concentration in the same ice core (Epifanio, et al., 2020).

The SPC14 ice core was drilled in 2014/15 over two field seasons and reached a depth of 1751 m. The SPC14 record spans the last 54,300 years (Winski et al., 2019, Epifanio et al., 2020). The data set provides a valuable context for better constraining the complex controls on TAC in ice cores. The record shows long-term and short-term variations (Figure 1) which would not be resolved without our high-resolution measurements. In the discussion below, we compare the TAC record to solar insolation curves, as well as a variety of known climate proxies. We present a simple linear regression that explains variability in our record as a function of insolation and several other proxies. Our study supports the insolation control on TAC but also shows that other firn densification-related processes create significant millennial-scale variability, underscoring the need for high-resolution data to use TAC records for constraints on gas trapping, ice core chronologies, and even past ice-sheet elevation changes.

2 Materials and Methods

2.1 Total air content measurements

The total air content (TAC) record from the SPC14 ice core was measured jointly in the Oregon State University (OSU) and Pennsylvania State University (PSU) ice core labs concurrently with measurements of CH_4. The core was discretely sampled at approximately 1- to 2-meter resolution. Methods followed previous work (Epifanio, et al., 2020, Mitchell et al., 2011, Lee et al., 2020, Buizert et al., 2021) with some calibration updates described below. At OSU, the samples were measured in accordance with previously published methods (Mitchell et al., 2015, Buizert et al., 2021). The PSU samples were also measured concurrently with CH_4, using a wet extraction system. The differences in methods between OSU and PSU wet extraction systems are described in Mischler et al., 2009, Fegyveresi, 2015, Epifanio et al., 2020, and WAIS Divide project members, 2013. Updates

to the methods at OSU allow a simple correction to the TAC measurements for variations in flask and array temperatures and volumes. The methods allowing this are described in detail below.

The OSU vacuum line is set up as portrayed in Figure 2. Samples are melted under vacuum in a two-sided array of twelve glass vacuum flasks. The air released during the melt step is trapped in the headspace of the flasks. The melted samples are then refrozen in a -70 °C ethanol bath. Once samples are refrozen, the air trapped in the flask headspace is expanded through the array volume, isolation volume and into the gas chromatograph (GC) sample loop. In the equations below, the quantity of air in the entire vacuum line (in moles) at this point is designated n_1. The relevant array valve is then closed, trapping air upstream of the isolation and GC volumes (Figure 2). This quantity of air is designated n_2. The pressure in the GC volume is recorded by a capacitance manometer (rated at 0-100 torr, 1.5% accuracy, P_1) The air in the GC sample loop is then injected into the GC column and measured for CH_4 concentration using a 6890N Agilent gas chromatograph with flame ionization detector. Once the analysis is complete, the gas remaining in the GC and isolation volumes (Figure 2) is evacuated. The remaining air from the relevant array is then expanded into the GC section, the relevant array valve is then again closed, trapping air upstream of the isolation and GC volumes (Figure 2). In total, we make four expansions and four measurements of CH_4 concentration, and four measurements of GC pressure per sample. We assume that the temperatures of the vacuum line and GC do not change during the repeated expansions. TAC is derived from the sample mass and pressure measurements during the analysis, following the ideal gas law:

$$n = \frac{PV}{RT_{eff}},$$
(1)

Where P is Pressure, V is volume, n is moles of air, T_{eff} is effective temperature (K) or weighted mean temperature of the various sections of the vacuum line, and R is the universal gas constant, 8.314 $J mol^{-1} K^{-1}$.

The effective temperature of the line can change from day to day due to differences in air temperature, ethanol bath temperature, chiller efficiency, and flask headspace variation due to sample size. Because of the daily variation, it is problematic to use a weighted average calculation of T_{eff} in our calculation of TAC, as this would require a daily estimate of T_{eff} or an assumption that it is constant. To avoid this issue, we take advantage of the methods for CH_4 measurement. During the CH_4 measurement, we expand the air released from the melted ice in four expansions, with each subsequent expansion releasing lower pressures from the flask headspace. The ratio between the subsequent expansion pressures allows us to calibrate the TAC measurement, as follows.

Deleted: and the remaining air in the array volume is again isolated as described above.

Deleted: subsequent

Deleted: i=

Deleted: 1

Deleted: /molK

Deleted: ¶

Deleted: fact that we do multiple expansions on the vacuum line to make multiple CH_4 measurements, and then use the ratio of expansion pressures to calibrate the TAC measurement, as follows.

Because the amount of air in the first expansion is equal to the amount in the second expansion plus what was removed by evacuation:

$$n_1 = n_2 + n_{rem} \qquad (2)$$

145

Where n_1 is the amount of air in the line during the first expansion, n_2 is the amount of air in the line during the second expansion, and n_{rem} is the amount of air removed in the first expansion, and:

$$n_1 = \frac{P_1 V_T}{R T_{eff}}, \; n_2 = \frac{P_2 V_T}{R T_{eff}}, \; n_{rem} = \frac{P_1 V_{gc}}{R T_{gc}} \qquad (3)$$

150

Where P_1 is the pressure of the first expansion, V_T is the total volume of the vacuum line and GC, and V_{gc} and T_{gc} are the volume and temperature of the vacuum line past the GC valve. Following from equation (2),

$$\frac{P_1 V_T}{R T_{eff}} - \frac{P_2 V_T}{R T_{eff}} = \frac{P_1 V_{gc}}{R T_{gc}} \qquad (4)$$

155

Rearranging to solve for $\frac{T_{gc}}{V_{gc}}$:

$$\frac{T_{gc}}{V_{gc}} = \frac{T_{eff} P_1}{V_T (P_1 - P_2)} \qquad (5)$$

160 and then rearranging to solve for T_{eff}

$$T_{eff} = V_T \frac{P_1 - P_2}{P_1} \frac{T_{gc}}{V_{gc}} \qquad (6)$$

TAC is calculated by dividing n_1 by sample mass. To eliminate the need to measure T_{eff} every time TAC is
165 calculated, we use Teff from equation 6 in the calculation of TAC:

$$\frac{n_1}{m} = \frac{P_1^2}{R(P_1 - P_2)} \frac{T_{gc}}{m V_{gc}} \qquad (7)$$

We then substitute R in equation (7) for the ideal gas law, with a final calculation for TAC:

170

$$TAC = \frac{P_1^2}{R(P_1-P_2)} \frac{T_{gc}T_{STP}}{mV_{gc}P_{STP}}$$
(8)

For comparison with previous work we convert to units of cm^3STPg^{-1}. Equation (8) requires that we have an accurate measure of $\frac{T_{gc}}{V_{gc}}$. Two separate methods were used to achieve this. The first method involved

175 estimating T_{eff} by taking a weighted average of the system temperature with the GC oven at 50 °C and the flasks submerged in a -70 °C ethanol bath. Once a known amount of air was expanded into the GC, $\frac{T_{gc}}{V_{gc}}$ was calculated. The line temperature for the portion outside the GC oven was estimated by averaging the measured temperature at multiple points adjacent to the line. The variation in temperature of the line was less than 0.1 °C. The final value of $\frac{T_{gc}}{V_{gc}}$ determined using this method was is 12.37 Kcc^{-1}.

180 The second calibration did not use the chilled flasks and instead utilized a removable known volume of air that was externally attached to the vacuum line. From expansions of air to other parts of the array and GC, we were able to calculate the volume of the entire system and individual components and the GC. All volumes are listed in Table 1. Air was expanded into the entire system at a known pressure, with the GC at room temperature (21.5 °C). The front array valve was closed, isolating the pressure in the front array, while the rest of the line was

185 pumped to vacuum. After the pressure stabilized, the air in the front array was expanded to the entire line, and the pressure was recorded. Finally, the GC oven was switched on and raised to the normal operating temperature (50 °C). The pressure in the total line after heating was recorded as P_{eff}. To solve for T_{eff}, we use the combined gas law:

190

$$\frac{P_1V_1}{T_1} = \frac{P_2V_2}{T_2}$$
(9)

Where $P_1 = P_{array}$ is the pressure of the air in the front array with the line at room temperature, $V_1 = V_{array}$ is the volume of the front array, T_1 is the measured lab temperature, $P_2 = P_{eff}$ or the pressure of the air in the entire system, including both array volumes, isolation volume, and the GC volume, and $T_2 = T_{eff}$ or the effective temperature of the entire system with the GC at 50 °C. Rearranging equation (9) to solve for T_2 (or T_{eff}):

195

$$T_{eff} = \frac{P_{eff} V_T T_{array}}{P_{array} V_{array}} \tag{10}$$

Finally, multiple expansions of air from the front array to the GC volume consistently give a ratio of pressures (between the four subsequent expansions for one measurement) of 0.56. Combined with equation (5), this ratio yields a final $\frac{T_{gc}}{V_{gc}}$ of 12.79 Kcc⁻¹. This value is different from the original value of 12.37 Kcc⁻¹ but we believe is more accurate due to the difficulty of estimating T_{eff} during the first calibration. The second method also removes the variability of flask size and accounts for small changes made in the vacuum line over time. All measurements of TAC on the SPC14 ice core were calibrated using the $\frac{T_{gc}}{V_{gc}}$ value of 12.79 Kcc⁻¹.

2.2 Solubility and cut bubble corrections

Two small corrections were made to the TAC measurements to account for effects on TAC introduced during sample preparation and measurement. Because the air trapped in the headspace of the flask is not allowed sufficient time to reach solubility equilibrium during the melt refreeze process, a correction was made to account for the residual gas trapped in the refrozen ice. Following Mitchell et al. (2015), we determined an empirical TAC solubility correction of +1.3 %, which we added to all sample measurements. This empirical correction was derived during wet extraction by measuring the TAC remaining within the flask headspace after a second melt-refreeze cycle.

The second correction accounts for the air lost during cutting and trimming the ice samples. Preparing ice-core samples for measurement unavoidably cuts through some bubbles, releasing a fraction of the air content from the entire ice sample. As a result, measurements made of the total air are slightly lower than true values.

This cut-bubble correction is based on a statistical relationship between the total number and average size of bubbles in a given sample, and the amount of exposed surface area that is cut during sample preparation (Saltykov, 1976). Bubble numbers and average sizes were determined during number-density, physical property, and micro-CT measurements as described in Fegyveresi et al. (2011), Fitzpatrick et al. (2014), and Fegyveresi et al. (2018). Following the methods in Matinerie et al., (1990) and Fegyveresi (2015), we interpolated the bubble size and density to each TAC sample, and applied the correction based on the bubble size distribution for each sample across the dataset. To estimate the exposed surface area of each sample, we used standard rectangular dimension (2.5 cm x 2.5 cm x 9 cm), and a mass of 51.2 g across all samples. There is likely some missed variation due to trimming on the edge of samples, but the variation is small. The cut-bubble correction indicates a maximum

250 of 8 % loss in the first 200 m of ice, decreasing to 1.9 % TAC loss at the base of the bubbly ice at ~1200m, at the onset of the clathrate-ice transition. The correction is shown in Fig. 3. While clathrate ice will still have a gas-loss correction, it is likely constant and no more than 1.9 %. We applied no correction below the base of the bubbly ice.

3 Results and Discussion

255 **3.1 South Pole total air content record**

The SPC14 ice core TAC record is shown in Fig. 1, plotted on the SPC19 ice age scale (Winski et al., 2019). We plot our data on the ice-age scale, rather than the gas-age scale, given evidence that ice-sheet surface conditions have a major impact on the pore volume at bubble close-off (further discussed below). This convention is consistent with previous research (Eicher et al, 2016, Raynaud et al, 2007). Using the method described above,

260 we measured TAC concurrently with the SPC14 CH$_4$ (Epifanio et al., 2020), resulting in a total of 2,318 measurements made on samples at 1,067 individual depths. Samples were taken at approximately every meter along the depth range from 131 m to 1,751 m, which spans the period of 130 to 54,302 years BP. The age resolution of these samples is the same as reported for CH$_4$ in the SPC14 ice core, averaging 42 years, but increasing from 20 years in the Holocene to 190 years at the bottom of the ice core record (Epifanio et al., 2020).

265 The OSU data set has a pooled standard deviation of 0.0006 cm^{-3}g^{-1} and the PSU data set (130-1150 m) has a pooled standard deviation of 0.002 cm^{-3}g^{-1}. Differences in methods between the OSU and PSU labs created a mean offset of 0.0072 cm^3/g. To correct for this offset, PSU values were increased to be comparable to OSU values. The pooled standard deviation of measurements for the combined dataset (130-1150 m) is 0.002 cm^{-3}g^{-1}, and data from 1151 – 1751 m have a pooled standard deviation of 0.001 cm^{-3}g^{-1}. Data are available at the USAP

270 data repository (https://doi.org/10.15784/601546) including the details of uncertainties and sample resolution of datasets (Epifanio, et al., 2022). To our knowledge, this is the first ice core TAC record with this resolution and length, allowing in-depth comparison with other climate proxies at a site that is not likely to have experienced significant elevation change over the last 54 ka (Fudge et al., 2020, Lilien et al., 2018).

The SPC14 TAC record has several notable characteristics (Figure 1). Long term trends include an

275 increase in TAC from 53 ka to 36 ka, followed by an approximately 10 ka period of low variability, then decreasing TAC from about 20 ka to the present. Millennial-scale variations, both in the Holocene and glacial period, consist of large magnitude abrupt changes. These variations are as large as 0.007 cm^{-3}g^{-1} in 2,600 years, which is 47 % of the total amplitude in the record. Higher frequency variations exist on centennial or shorter timescales that may

represent firn processes such as layering, but our sampling resolution is not adequate to fully evaluate this possibility.

3.2 Impacts of temperature on TAC

295 Prior work suggests that temperature impacts TAC in two ways, the first through the ideal gas law, and the second through an empirically established relationship between the pore volume at bubble close-off and temperature (Martinerie et al., 1992). Given a fixed pore volume at close-off, TAC is given by the ideal gas law:

$$TAC = V_c * \frac{P_c}{T_c} * \frac{T_0}{P_0}$$ (11)

300 Where TAC is the total air content ($cm^{-3}g^{-1}$), V_c is the pore volume at close off ($cm^{-3}g^{-1}$), P_c and T_c are pressure and temperature of the air contained in V_c at close-off (mb and K), and P_0 and T_0 are standard pressure and temperature (1013 mb and 273 K, respectively).

The empirical relationship between pore volume and temperature, as found by Martinerie et al. (1992) is
305 given by:

$$V_c = 7.6x10^{-4} * T_s - 0.057$$ (12)

Where T_s is the surface temperature (K).
310

To examine direct thermal effects, we follow Raynaud et al. (2007) and Eicher et al. (2016) to define a non-thermal residual term V_cr:

$$V_{cr} = TAC * \frac{T_c}{P_c} * \frac{P_0}{T_0} - V_c$$ (13)

We use the same temperature for the surface (T_s), and the close-off depth (T_c). While the temperature at
315 pore close-off (T_c) is a bit warmer than T_s due to geothermal heating, the difference is small when the firn column is in equilibrium. For the temperature at bubble close-off (T_c), we used a temperature reconstruction from Kahle et al (2021). To approximate P_c, we use value of 680 mb at the surface of the ice core, linearly decreasing with depth to account for 180 m of elevation increase upstream of the drill site (NOAA GML, 2020, Fudge et al., 2020).

Following Raynaud et al. (2007) and Lipenkov et al. (2011), we then create standardized versions of TAC and V_{cr}, called TAC* and V_{cr}*, in order to compare TAC and the non-thermal residual. The standardized data sets were created by subtracting the mean value (of TAC or V_{cr}, respectively) and then dividing by the respective standard deviation. These data are plotted together in Fig. 4. The correlation between TAC* and V_{cr}* is very high ($r^2 = 0.96$). Because V_{cr}* is a quantity that describes TAC, if temperature did not affect pore volume at close-off, and is useful for understanding the magnitude of the direct effects of temperature. The very high correlation between TAC* and Vcr* agrees with previous work on both EDC and NGRIP ice cores that show the direct temperature effect on TAC is responsible for a very small amount of TAC variability. As a result, we targeted our analysis using measured TAC instead of the non-thermal residual.

3.3 Orbital-scale variations in TAC

Local integrated summer insolation (ISI) has shown an anti-correlation with TAC in various Antarctic and Greenland ice cores (Raynaud et al., 2007, Lipenkov et al., 2011, Eicher et al., 2016). South Pole is an interesting site to study in this regard, as it is the only place in Antarctica without a diurnal cycle in solar insolation. Following Huybers et al. (2006) and Raynaud et al. (2007) we find ISI by:

$$ISI = \sum \beta_i (\omega_i * 86,400) \tag{14}$$

where ISI is in joules, ω_i is the daily insolation in Wm^{-2}, and β_i is a Heaviside step function, where $\beta_i = 1$ when ω_i is $> \omega_{threshold}$, otherwise $\beta_i = 0$. ISI is impacted by a mix of precession and obliquity and the curves are unique for latitude and the chosen $\omega_{threshold}$.

Earlier research emphasized the anti-correlation between ISI and TAC and uses the relationship to orbitally tune the ages of Antarctic ice core records (Lipenkov et al., 2011, Raynaud et al., 2007, Parrenin et al., 2007). Conclusions of previous work suggest that the insolation effect is much larger than the direct effects of temperature discussed above and is found in both Northern and Southern Hemisphere records (Eicher et al., 2016).

We find a maximum anti-correlation of ISI with TAC at a cutoff threshold of 225 Wm^{-2} ($r^2 = 0.46$, p < 0.0001). Studies of the same relationship in the EDC and NGRIP ice cores found maximum correlations at different cutoff values (390 Wm^{-2} for NGRIP with $r^2 = 0.3$) (Eicher et al., 2016, Raynaud et al., 2007). However, the correlation difference between varying threshold values (0 to 500 Wm^{-2}) is small ($r^2 = 0.42$ to $r^2 = 0.46$). The linear regression of TAC as a function of ISI at a threshold cutoff of 225 Wm^{-2} is shown in Fig. 5. To make this calculation, we interpolated the ISI data to the ages assigned to TAC.

375 The ISI regression misfit values show an even distribution. The link between TAC and ISI supports the proposition that TAC can be used for absolute (orbitally tuned) dating of ice cores (Raynaud et al., 2007). It is worth noting, however, that the SPC14 TAC record only covers the last 54,000 years, which is only slightly longer than one obliquity cycle. This time period is shorter than the ice core records mentioned above, which may affect the differences in cutoff threshold that give maximum correlation between TAC and ISI.

3.4 Millennial-scale variations observed in TAC

380 While the ISI appears to be highly correlated with long-term variations in TAC, it fails to explain the observed millennial-scale changes. Abrupt, large magnitude, millennial-scale variations in TAC exist through the Holocene and early part of the glacial period. The approximate magnitude of the largest, abrupt. millennial-scale changes is 0.007 cm^3g^{-1} in ~ 3 kyr, which is similar to the abrupt millennial-scale variations observed in NGRIP, which were typically around 0.01 cm^3g^{-1} in the same time frame (Eicher et al., 2016). Millennial-scale variations

385 are absent from 40 ka to 22 ka in the SPC14 ice core, but high frequency (centennial-scale and smaller) variations persist through the entire record. The existence of millennial-scale and higher frequency variations underscores the need for high-resolution data to discern the long-term patterns from other climatic effects on TAC. We isolate the millennial-scale TAC variations by subtracting the orbital-scale trends that we find via regression of TAC onto ISI (Figure 5). The largest millennial-scale features occur at 52 ka, 46 ka, and 44 ka. Similar large features are not

390 found between 43 ka and 25 ka, where the TAC reaches a maximum, steady value of about 0.11 cm^3g^{-1}. Large variations resume at 22 ka and occur through the Holocene time period, mostly between 9 ka and 2 ka.

We first investigate the possibility of surface pressure changes driving the millennial-scale variability. Using the relationship of air pressure with TAC (Eq. 11) as proposed by Martinerie et al., (1992), we calculated the pressure change required for a representative high-frequency TAC change. For example, the abrupt increase

395 in TAC of 0.01 cm^3g^{-1} in 2.7 kyr starting at 49.2 ka (Figure 1) would require a mean pressure change of 104 hPa over that time interval. In the absence of elevation change, central Eastern Antarctica could not likely sustain large atmospheric pressure changes for that length of time. Hourly atmospheric pressure measurements at the South Pole are between 710 and 650 hPa, varying on seasonal timescales (NOAA GML, 2020). However, daily, or even seasonal, variations in pressure are not likely to be recorded in our TAC record due to the gradual bubble trapping

400 process that takes decades to complete. Current spatial gradients of sea level pressure, including variations associated with the Amundsen Sea Low (ASL), show a maximum range of about 50 mb from maximum low to high pressure over Antarctica (Schneider et al., 2012, Raphael et al., 2016). A change in atmospheric pressure large enough to explain these TAC variations would require a dramatic reorganization of the westerly winds,

which is highly unlikely during the last glacial period. Some modeling studies have examined wind changes around Antarctica, using 10,000-year model runs, and found moderate changes in sea level pressure, no greater than 15 hPa (Goodwin et al., 2014). The wind effect, as described in Martinerie et al. (1994) would require large, sustained wind changes over millennia that are not supported by modeling reconstructions (Goodwin et al., 2014).

415   If the TAC change were entirely explained by a surface pressure change induced from ice sheet elevation changes, an elevation change of about 1,200 meters would be needed. Such a large and abrupt change is unlikely to have been driven by accumulation change alone and is otherwise not likely due to the geographical context of the South Pole. Accumulation rates during the glacial period were just 3 cm yr^{-1} (water equivalent), which would mean the maximum amount of elevation gain due to accumulation alone would be only about 80 meters, without

420   considering the effects of ice layer thinning.

The location of SPC14 In the interior of Eastern Antarctica means that it would not have been subject to large elevation changes associated with major climate transitions, especially during the beginning of the last glacial period (Golledge et al., 2014, Fudge et al., 2020). The SPC14 ice core was not drilled at an ice divide, which means the ice collected at the South Pole flowed over topography before it arrived at the sampling location.

425   This flow changed the local elevation at which the snow fell in the past. The history of ice flow of the SPC14 ice core, however, is not constrained beyond 100 km from the core site and is best constrained in the closest 65 km, representing the last 10 ka, or about 725 m ice core depth (Lilien et al., 2018, Fudge et al., 2020). Following the ice flow line upstream from the modern ice core site shows the bedrock elevation only varying by about 500 m, which corresponds to an ice surface elevation variation of about 300 meters during that time (Lilien et al., 2018,

430   Fudge et al., 2020, Kahle et al., 2021, Morgan et al., 2022). This 300 m change is much less than the 1200 m change required by our millennial-scale TAC observations. Large transient features in surface ice sheet elevation do not exist, eliminating ice flow as a source of abrupt elevation change influencing TAC.

Other hypotheses for changing TAC include layering due to melt, and dust affecting grain metamorphism. Layering due to melt or other effects influences the trapping of air in ice, shaping TAC but is not

435   relevant here due to the lack of melt layers. Dust has also been documented to influence grain metamorphism in the firn. Due to its interior location, the ice at South Pole experiences very small changes in dust flux. We observe. No correlation between dust deposition and TAC.

3.4.1 Accumulation

Since we can reasonably show that large millennial-scale changes in TAC are not due to direct effects of

440   temperature, variations in air pressure or ice dynamics, pore volume at bubble close-off must account for most of

---

the TAC variations. Two observations are important to help explain these changes as a function of pore volume at close-off: (1) a positive correlation between TAC and accumulation rate, and (2), a high positive correlation between TAC and $\delta^{15}N$-N_2 in trapped air in the core.

First, the millennial-scale changes in TAC are highly correlated with the accumulation rate reconstruction from Kahle et al. (2021), also plotted on the SP19 ice age ($r^2 = 0.59$, p < 0.001, Figure 6 and Table 2). Kahle et al. (2021) calculated the accumulation rate by using an inverse method which used models of firn densification, water isotope diffusion, and layer thinning to predict an accumulation rate history based on constraints provided by measured Δage, diffusion length, and annual layer thicknesses. The first 11.3 ka of the Kahle et al. (2021) reconstruction incorporates measured annual layer thicknesses from the layer counted time scale from Winski et al., (2019). This results in an accumulation record that closely resembles the previous accumulation rate history from Winski et al. (2019) for this section of the core.

Second, the millennial-scale changes in TAC are also highly correlated with $\delta^{15}N$-N_2 when plotted on the SP19 gas age scale ($r^2 = 0.51$, p < 0.001, Figure 6 and Table 2). This observation is consistent with the idea that millennial-scale fluctuations in accumulation drive similar-scale changes in firn thickness, which affects $\delta^{15}N$-N_2 due to gravitational fractionation (Severinghaus et al., 1998, Sowers et al., 1992, Morgan et al., 2022). As temperature variations are relatively minor at the South Pole, it is accumulation variation that drives the observed changes in SPC14 $\delta^{15}N$-N_2. At this site, greater accumulation rates causing a thicker firn column and a subsequently higher $\delta^{15}N$-N_2. Because $\delta^{15}N$-N_2 is not set until pore close-off, toward the base of the firn, comparison of the effect in $\delta^{15}N$-N_2 with accumulation rate is done using the gas age scale for $\delta^{15}N$-N_2 and the ice age scale for TAC. Winski et al. (2019) also notes the close resemblance of $\delta^{15}N$-N_2 and the Holocene accumulation rate reconstruction, which is further evidence to support the use of $\delta^{15}N$-N_2 as an indicator of accumulation rate changes in SPC14. TAC was compared with temperature reconstructions as well as $\delta^{18}O_{ice}$. Low r-values were recorded, and the results are listed in Table 2. Note that Kahle et al. (2021) do not use the $\delta^{15}N$-N_2 in their inversion method.

Metamorphism of the ice in the first few meters of the firn may explain the link between accumulation rate and TAC. Lower accumulation rates allow grains to remain at or near the surface for a longer time, giving grains in the firn more time to grow while they remain at the surface (Courville et al., 2007). The size of the firn grains at the surface seems to predict at which density bubble close-off occurs, with larger grained firn closing off at a higher density (Arnaud, 1997, Gregory et al, 2014). Because ice density is, by definition, inversely proportional to porosity, higher density bubble close-off (associated here with longer time near the surface of the ice sheet, larger grain sizes, and lower accumulation) leads to bubbles with less pore volume than firn with smaller grain sizes. Lower accumulation rates may additionally allow more time for grains to become spherically shaped,

510 before close-off, where higher accumulation rates tend to close off bubbles earlier in the densification process. Because grains tend to move toward a spherical shape with enough time, due to vapor diffusion (Eicher et al., 2016), low accumulation rates create more homogeneous, spherically shaped grains. These spherically shaped grains could force more air to escape the ice core, leading to lower TAC. (Gregory et al., 2014) noted higher gas diffusivity at lower accumulation sites, implying that at low accumulation sites, the pores are closing off later,

515 allowing time for more spherically shaped grains. We propose that a mechanism of grain size and shape affecting pore volume leads to a positive correlation between accumulation and TAC, which we observe in the SPC14 ice core, however the microstructure and physics behind the mechanism should be explored in future work.

In a sense this proposed grain size mechanism is similar to the proposed mechanism for how ISI impacts TAC on an orbital time scale (Raynaud et al., 2007, Eicher et al., 2016). ISI is hypothesized to act on TAC by

520 changing the grain size of the firn at the surface by influencing temperature gradients in the first few meters of firn. On orbital timescales, higher ISI increases the near-surface firn metamorphism and grain size, and decreases pore volume at close off, resulting in the inverse relationship between TAC and ISI recorded in both hemispheres (Raynaud et al., 1997, Eicher et al., 2016). In our proposed mechanism for millennial-scale variations in TAC, lower accumulation increases near-surface firn metamorphism and grain size and decreases pore volume at close-

525 off. In both scenarios (orbital- and millennial-scale changes), grain size is set in the first few meters of the firn, though by different mechanisms, and the impact is advected to the close-off depth. We propose that the relationship between grain size and accumulation rate is responsible for the large, millennial-scale changes in TAC found in the SPC14 ice core. This mechanism is complimentary to the orbital changes in TAC imposed by ISI and creates millennial-scale changes imposed on top of orbital-scale changes.

530 Studies of TAC in Greenland suggest a different mechanism for similar-magnitude changes in TAC. Eicher et al. (2016) observed a complex, asynchronous relationship between rapid climate changes (D-O events) and millennial-scale TAC changes in the NGRIP ice core. Figure 7 shows the Greenland (North GRIP) TAC record compared with accumulation at the same site. Eicher et al. (2016) suggest the relationship is due to step changes in accumulation rate and temperature during D-O events in Greenland, causing the firn to densify rapidly

535 due to increased load changes. This hypothesis is not consistent with our results in the SPC14 ice core, perhaps because the load changes in Antarctica are not nearly as large or abrupt as observed in Greenland. Accumulation rate changes at the South Pole during the glacial period are much smaller than in Greenland (1 cm yr^{-1} or 25 % change over an AIM event, compared with 10 cm yr^{-1} or 100% increase during a D-O event in Greenland), while the TAC changes at both locations are of a similar magnitude (0.007 cm^{3}g^{-1} at SPC14, 0.005 cm^{3}g^{-1} at NGRIP).

540 This suggests that the accumulation effect on TAC scales differently at NGRIP when compared to SPC14,

Deleted: L

Deleted: which

Deleted: .

Deleted: H

Deleted: accumulation rate and

Deleted: They

Deleted: .

Deleted: /yr

Deleted: /yr

Deleted: cm^3/g

Deleted: cm^3/g

implying that the two locations respond differently to accumulation changes. Interpreting TAC at any ice core requires a universal explanation of how the firn densifies, and future work may elucidate a single mechanism that can explain the TAC-accumulation relationship at both polar regions. For example, we hypothesize that the grain size mechanism dominates at colder, dryer locations, and the mechanism requiring transient firn densification would prevail when warmer, wetter conditions exist. High resolution TAC datasets across a suite of climate conditions are needed to test this hypothesis.

3.5 Multiple regressions to further investigate controls on TAC

A multiple-regression analysis was performed to examine how climate-related variables correlate with TAC at SPC14. This analysis was performed to examine the possibility of removing non-elevation-dependent signals the record. Because we do not expect large elevation changes at the South Pole site, SPC14 is an excellent ice core to examine this possibility. If the TAC variability in the SP14 core can be explained using measured or modeled climate variables, it might be possible in future projects to extract the portion of the variability due to elevation change. Here we considered two separate multiple linear regression analyses. In the first multiple regression (referred to as the 'modeled reconstruction' regression), we examined the relationship between TAC, ISI, and accumulation rate. In the second multiple regression (referred to as the 'measured data' multiple regression), we examined the links between TAC, ISI, and δ^{15}N-N$_2$. TAC data and variables considered are plotted in Figure 8.

The modeled reconstruction regression included TAC, ISI, and the Kahle et al. (2021) reconstruction of accumulation rate. The modeled reconstruction multiple regression had a maximum adjusted r^2 = 0.51, (p < 0.0001), therefore the combined relationship accounts for 51% of the variation in the SPC14 TAC. The modeled reconstruction multiple regression residuals show an even distribution. The parameters are listed in Table 3 in order of how much each parameter affected the adjusted correlation coefficient.

The regression using only measured parameters incorporated δ^{15}N-N$_2$ instead of using the modeled accumulation rate. Results are listed in Table 3. We find a maximum adjusted r^2 = 0.62 (p < 0.0001). Both the modeled and measured parameter multiple regressions compare well (Figure 9).

For both the modeled and measured regression models, addition of other climate variables increased the goodness of fit. Adding temperature and Δage to the modeled multiple regression increased the r^2 to 0.72. Adding δ^{15}N-N$_2$ and δ^{18}O$_{ice}$ to the measured parameter multiple regression increased the r^2 to 0.69. While adding these parameters increased the goodness of fit of the models, suggesting that they do record phenomena important to

controlling TAC, the other climate parameters are also highly correlated between themselves, which makes the interpretation of the regression parameters difficult (Gregorich et al., 2021).

Large misfits between the multiple regression solution and measured TAC seem to occur during times when the climate is rapidly changing. An interesting feature of this analysis is that if the derivative of Δage (dΔage/dt) is added to the multiple regression, it seems to explain more of the variability observed in the TAC record. A comparison between a regression that includes dΔage/dt, and a regression that does not is shown in Figure 9. Specifically, dΔage/dt seems to correlate well with the magnitude of TAC change that occurs at 2,600 years as well as the large variations that occur between 45 ka and the oldest part of the record. A regression analysis that includes the dΔage/dt and the measured parameters (ISI, $\delta^{15}N$-N_2, $\delta^{18}O_{ice}$, and Δage) gives an adjusted r^2 of 0.77 (p < 0.0001), meaning that the dΔage/dt and its interactions describe about 8 % of the measured data multiple regression solution. Adding dΔage/dt to the modeled reconstruction multiple regression increases the r^2 adjusted by 4 %.

A possible explaination for why dΔage/dt explains this extra variation is that Δage responds to changing climate conditions, and times when Δage is changing rapidly (large dΔage/dt) correspond with large changes in temperature and accumulation rate not tracked adequately with other variables. We specifically observe this at D-O 12 and 13. This agreement between large dΔage/dt and rapid climate changes again points to a mechanism in the firn column that responds to transient accumulation changes. Following the reasoning of Eicher et al. (2016), times of large changes in accumulation may not allow the firn to form spherical bubbles, creating less pore space, and therefore lower TAC values.

An observation that is not explained by the multiple regression is the apparent lack of TAC variability from around 25 ka to 42 ka. This section of the record seems to stop responding to millennial-scale forcing. In fact, our multiple regression predicts millennial-scale changes during this time that are not realized in the TAC record, most notably a large, predicted change around 32 ka that is not reflected in TAC. A possible explaination for the lack of variation could be that the effect of accumulation rate on TAC is inhibited when ISI is at a minimum. This inhibition of accumulation effects on grain size could be due to ISI dominating the grain metamorphism mechanism during that period. However, more detailed studies including high resolution TAC through multiple orbital cycles would be needed to address this question.

An interesting feature of this analysis is that if the derivative of Δage (δΔage/δt) is added to the multiple regression, it seems to explain more of the variability observed in the TAC record. A comparison between a regression that includes δΔage/δt, and a regression that does not include δΔage/δt is shown in Figure 8. Specifically, δΔage/δt seems to correlate well with the magnitude of TAC change that occurs at 2,600 years as well as the large variations that occur between 45 ka and the oldest part of the record. A regression analysis that includes ∂Δage/∂t and the measured parameters (ISI, δ¹⁵N-N₂, δ¹⁸O_ice, and Δage) gives an adjusted r² of 0.77 (p < 0.0001), meaning that δΔage/δt and its interactions describe about 8% of the measured data multiple regression solution. Adding δΔage/δt to the modeled reconstruction multiple regression increases the r² adjusted by 4%. While the reason δΔage/δt helps explain TAC changes in the firn is not at first clear, times when δΔage/δt are large occurs at the same time as large changes in temperature and accumulation rate, specifically at D-O 12 and 13. This points to a mechanism in the firn column that responds to transient accumulation changes. Following the reasoning of Eicher et al (2016), times of large changes in accumulation may not allow the firn to form spherical bubbles, creating less space, and therefore lower TAC values.

4 Conclusion

We present a high-resolution total air content record from the SPC14 ice core covering the last 54 kyr. The implications of the analysis of the SPC14 TAC record are twofold. First, this study strongly confirms previous research on Greenland (NGRIP and GRIP) ice cores as well as Antarctic ice cores (EDC) that low-frequency variations in TAC depend on local summer insolation. Importantly, the high correlation with integrated summer insolation (ISI) corroborates the potential to orbitally tune ice age scales using TAC. Second, because the SPC14 ice core was drilled at a location with relatively small expected elevation changes over the course of the ice core history, it provides a good location to study controls on TAC outside the influence of elevation changes. Our results suggest that temperature, accumulation rate, and other firn column properties interact together to affect TAC and provide important context for developing paleoelevation proxies in cores that may have experienced large elevation changes.

We propose that a common mechanism, grain size metamorphism in the top few meters of the firn, can explain both orbital and millennial-scale times scale of TAC variations in the SPC14 ice core. Although our data are consistent with an orbital scale impact of ISI on TAC, and an accumulation-driven millennial component, further work is needed. Future directions should include:

(1) High-resolution sampling of TAC in multiple ice cores. High-resolution data are required to resolve all millennial-scale features in TAC. These features need to be accounted for before applications like paleoelevation constraints are useful. Data should be collected for both Northern and Southern Hemisphere ice cores, and at a variety of accumulation rate regimes.

(2) Further understanding of links between $\delta^{15}N\text{-}N_2$, Δage, and TAC in ice cores. Accumulation rate can influence the $\delta^{15}N\text{-}N_2$ and Δage depending on climate, and therefore influence the TAC differently at different sites. High-resolution sampling of $\delta^{15}N\text{-}N_2$ in ice cores, and model-independent Δage determinations, could be used in future work to corroborate findings from the SPC14 ice core. Additionally, TAC sampling at locations with well-known accumulation rate histories will provide further constraints.

(3) Comparison of TAC in regions that have stable elevation histories to regions with unstable elevation histories. Ice cores targeted in coastal regions with hypothesized unstable elevation histories, such as in Western Antarctica, should be targeted for future TAC research.

Data Availability

710   The SPC14 total air content record is published on and can be accessed through the USAP Data Center with DOI: https://doi.org/10.15784/601546.

Author Contributions

715   JAE, EJB, JSE, TAS, JPS, JMF, ECK contributed data to this study. JAE, EJB, CB, JSE, TAS, measured ice core gases. ECK and JPS made isotope measurements. JMF made bubble density and size measurements. EJB and TAS provided funding acquisition for the study. JAE, EJB, ECP, CB, JSE, JMF, JPS, wrote, reviewed and edited the paper with input from all authors.

720   ## Competing Interests

The authors declare that they have no conflict of interest.

Acknowledgements
725

This work has been funded by the National Science Foundation (Awards 1643722, 1443472, and 1443464). We would like to thank Mark Twickler and Joe Souney for their work administering the SPICEcore project; the U.S. Ice Drilling Program for collecting the SPC14; the field team who collected the ice core; the National Ice Core Facility for ice core storage and processing; Michael Kalk for his help on lab work with the samples, and the many 730   student researchers who produced data from the SPC14 ice core.

735
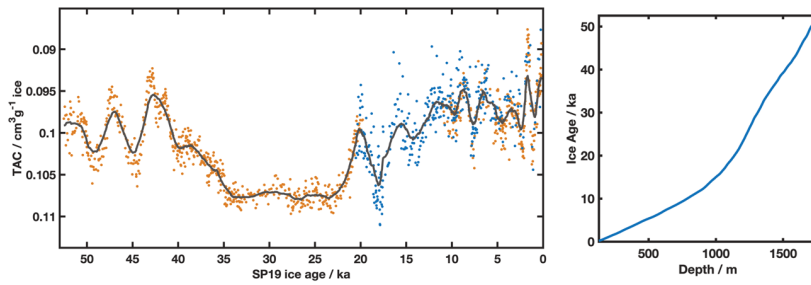
Figure 1: Total air content of the SPC14 ice core. (Left) Measurements are individually shown, plotted on the SP19 ice age scale (Winski et al., 2019). Black line is the smoothed record using a running 10-point average. TAC is expressed in units of cm^3 air at standard temperature and pressure, per gram of ice. Orange markers are TAC measurements collected at OSU (depths 130 – 841m, 1150-1751 m, pooled standard deviation = 0.0006 cm^{3}g^{-1}). Blue markers are TAC measurements collected at PSU (depths 130-1150 m, pooled standard deviation = 0.002 cm^{3}g^{-1}). (Right) Ice age as a function of depth. Data from Winski et al. (2019).
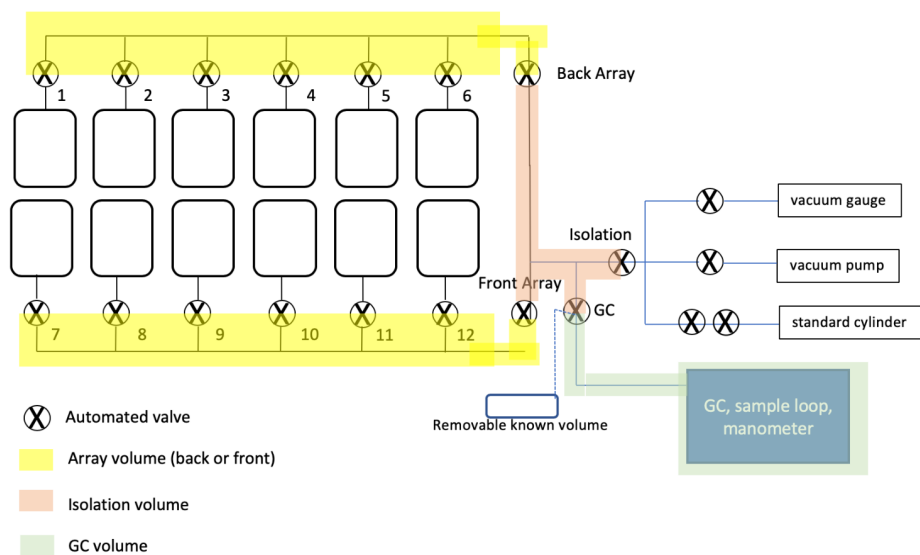
755 **Figure 2: Schematic of extraction line and GC for TAC and CH₄ measurements.** Diagram includes a removable known volume, which was used in the T_{eff} calibration (see text). Numbered valves are individual flask valves. Air released during the melt phase is trapped between the flask and the numbered automated valve. Yellow: Back and front array volumes. Light Orange: Isolation volume, includes the vacuum line between the array valves, the isolation valve, and the GC valve. Green: GC volume, includes the vacuum line between the GC valve and the GC sample loop. All volumes are listed in Table 1.

760
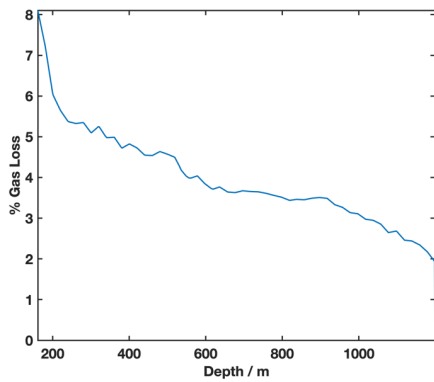
765

770

775 **Figure 3: Cut bubble correction for SPC14 ice core.** Gas loss plotted with depth on the SPC14 ice core. Cut bubble
corrections range from 8 % decreasing to 1.9 % gas loss at the base of the bubbly ice.

780

785

none
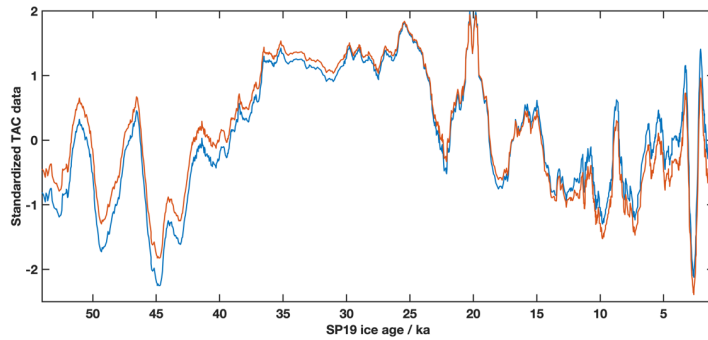
Figure 4. Comparison of TAC and the non-thermal residual. The non-thermal residual quantity, explained in section 3.2, explains how much temperature affects TAC. The TAC and non-thermal residual are nearly identical, indicating a very small direct effect of temperature on TAC. Blue: A standardized version of the SPC14 TAC record. Orange: Following Raynaud et al. (2007), the standardized TAC data after correcting for the direct effects of temperature (V_{cr}) (Martiniere et al., 1992). Both records were smoothed using a 10-point moving average, to better highlight the difference.
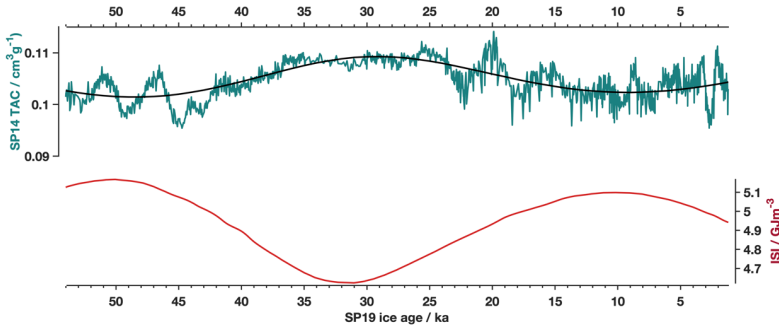
Figure 5: SPC14 TAC predicted from integrated solar insolation (ISI) Top: SPC14 TAC (green) and by linear regression of TAC with ISI using a cutoff threshold of 225 Wm^{-2}. $R^2 = 0.46$, $p < 0.0001$, b = 0.194, m = -0.0173. Bottom: ISI at 90 °S using a cutoff threshold of 225 Wm^{-2}.

820

825
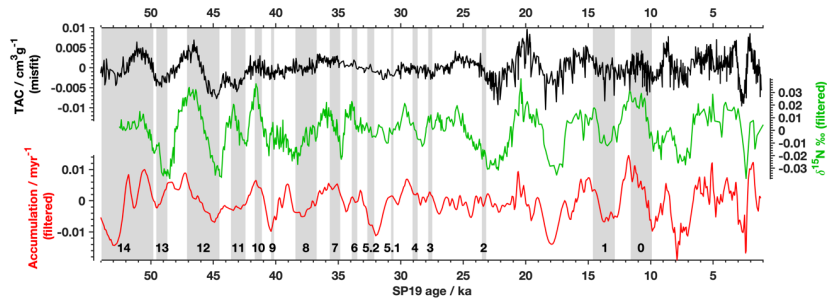
830

Figure 6: TAC, accumulation rate, and $\delta^{15}N$-N_2. TAC misfit (black, upper) compared with $\delta^{15}N$-N_2 (green, middle: Winski et al. (2019) accumulation rate (red, bottom: Kahle et al., 2021). Both the $\delta^{15}N$-N_2 data and accumulation rate and were filtered using a highpass filter removing variability with period greater than 10,000 years prior to comparison. TAC misfit was plotted on the SP19 ice age scale. The highpass filtered $\delta^{15}N$-N_2 is plotted on the SP19 gas age scale (Middle: Epifanio et al., 2019). The highpass filtered accumulation rate on the SP19 ice age scale (Bottom: Winski et al., 2019) Grey shaded areas are D-O events, numbered on the bottom for reference. Correlation coefficients are presented in Table 2.

Figure 7: TAC and Greenland (NGRIP) TAC. TAC (grey, upper: Eicher et al., 2016) compared with
accumulation rate (red, bottom: Kindler et al., 2014) Black line is smoothed TAC using a 10-point running
average. Grey shaded areas are D-O events, numbered on the bottom for reference. Correlation coefficients are
presented in Table 4.

875
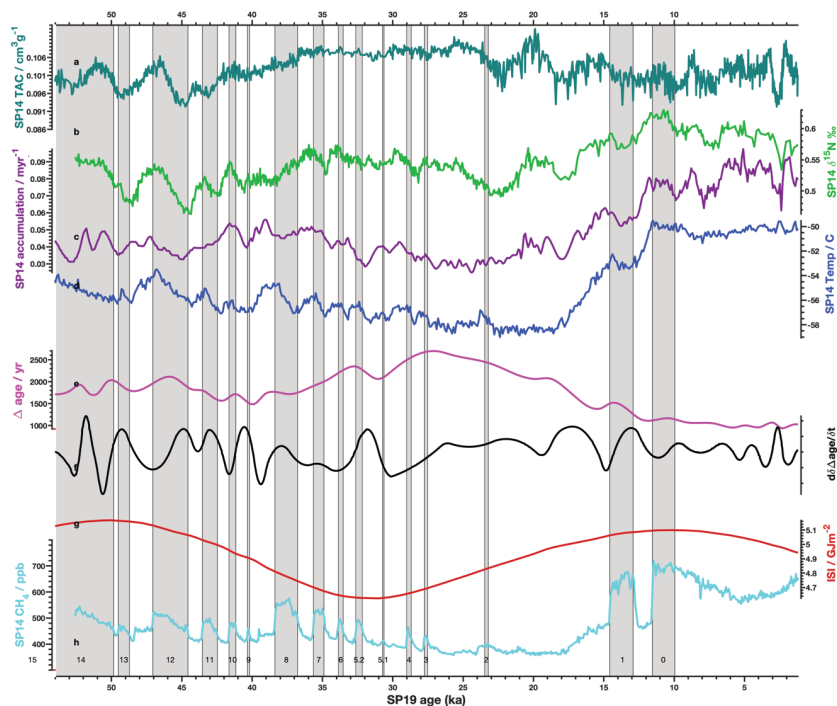
Figure 8: TAC record of SPC14 ice core and other climate proxies. a) SPC14 TAC record. Mean value of duplicate measurements, plotted on the ice age scale. b) $\delta^{15}N$-N_2, plotted on the gas age scale (Winski et al., 2019). c) Accumulation rate plotted on the ice age scale. For the last 11.3 ka the accumulation rate was constrained by layer counting of seasonal variations of magnesium and calcium ions (Winski et al., 2019). For older time periods, accumulation is modeled using an inverse method (Winski et al., 2019, Kahle et al., 2021). D) $\delta^{18}O_{ice}$ a local temperature proxy (Kahle et al., 2021). e) SPC14 Δage, empirically derived using independent gas and ice age markers (Epifanio et al., 2020) f) Derivative of Δage. g) Integrated Summer Insolation (ISI), at a cutoff threshold of 225 Wm^{-2}, at 90 °S (Huybers et al., 2006). h) SPC14 CH_4, plotted on the gas age scale, added for chronological orientation (Epifanio et al., 2020). Grey bars are numbered and represent D-O events for reference.
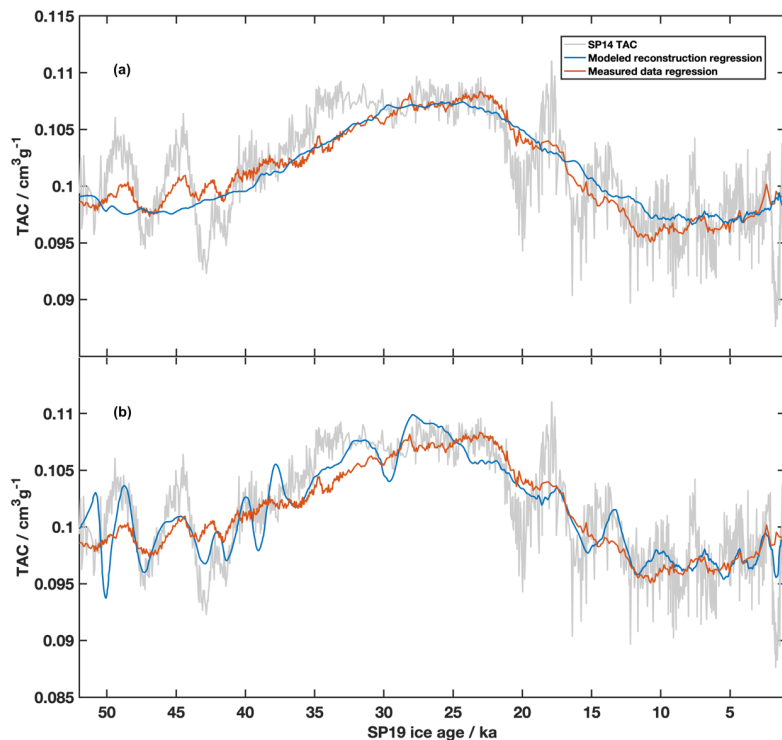
Figure 9: Multiple regressions of TAC compared to SPC14 TAC record. a) SPC14 TAC data (grey), modeled reconstruction multiple regression which used ISI and modeled reconstructions of accumulation rate ($r^2 = 0.51$, $p < 0.001$) (blue), measured data multiple regression which includes $\delta^{15}N\text{-}N_2$ and ISI ($r^2 = 0.62$, $p < 0.001$) (orange). b) Multiple regression comparison including $\delta\Delta$age/δt. SPC14 TAC data (grey), multiple regression using modeled reconstructions of temperature and accumulation rate, including $\delta\Delta$age/δt ($r^2 = 0.76$, $p < 0.001$) (blue), multiple regression using measured parameters including $\delta\Delta$age/δt ($r^2 = 0.77$, $p < 0.001$) (orange).

895

Table 1: Volumes of CH₄ extraction line. Volumes of CH₄ extraction line. Volumes listed correspond to highlighted areas in figure 2.

930

Line	Volume (cc)
Removable Known Volume	22.14
Front Array	28.45
Total	65.03
GC to isolation space	16.90
Isolation Space	6.19

Table 2: Pearson correlation coefficients of single regressions. Pearson correlation coefficients of single regressions.

935   Highpass filtered records were filtered using a bandpass filter than eliminated frequencies greater than 10,000 years.

	TAC	Highpass filtered TAC
$\delta^{15}N\text{-}N_2$	0.13	0.25
$\delta^{15}N\text{-}N_2$ (highpass)	0.25	0.51
Accumulation	-0.20	0.18
Accumulation (highpass)	0.18	0.59
$\delta^{18}O_{ice}$	-0.39	0.10
$\delta^{18}O_{ice}$ (highpass)	0.11	-0.13
Temperature	-0.37	0.11
Temperature (highpass)	0.11	0.05

940

Table 3: Multiple regressions of TAC Parameter listed is the term considered in the regression. Parameters are listed in the order of how much adjusted r^2 changes when the parameter is removed from to the regression. Left: terms of multiple regression of TAC, when using modeled reconstructions for temperature and accumulation rate ($r^2 = 0.51$) Right: terms of multiple regression of TAC when using measured parameters ($r^2 = 0.62$).

Modeled reconstruction multiple regression		Measured parameter multiple regression	
Parameter	**% Change in adjusted r^2**	**Parameter**	**% Change in adjusted r^2**
ISI	27	ISI	40
Accumulation	3	$\delta^{15}N$-N_2	13

References

Arnaud, L., Modélisation de la Transformation de la Neige en Glace à la Surface des Calottes Polaires; étude du Transport des gaz dans ces Milieux Poreux, PhD. Université Joseph Fourier, tel-00709566, version 1 (19-06-2012), 1997.

Arnaud, L., Barnola, J. M., and Duval, P.: Physical modeling of the densification of snow/firn and ice in the upper part of polar ice sheets, in: Physics of Ice Core Records, pp. 285-305. Hokkaido University Press, http://hdl.handle.net/2115/32472, 2000.

Bazin, L., Landais, A., Lemieux-Dudon, B., Toyé Mahamadou Kele, H., Veres, D., Parrenin, F., Martinerie, P., Ritz, C., Capron, E., Lipenkov, V., Loutre, M.-F., Raynaud, D., Vinther, B., Svensson, A., Rasmussen, S. O., Severi, M., Blunier, T., Leuenberger, M., Fischer, H., Masson-Delmotte, V., Chappellaz, J., and Wolff, E.: An optimized multi-proxy, multi-site Antarctic ice and gas orbital chronology (AICC2012): 120–800 ka, Clim. Past, 9, 1715–1731, https://doi.org/10.5194/cp-9-1715-2013, 2013.

Buizert, C., Fudge, T. J., Roberts, W. H. G., Steig, E. J., Sherriff-Tadano, S., Ritz, C., Lefebvre, E., Edwards, J., Kawamura, K., Oyabu, I., Motoyama, H., Kahle, E. C., Jones, T. R., Abe-Ouchi, A., Obase, T., Martin, C., Corr, H., Severinghaus, J. P., Beaudette, R., Epifanio, J. A., Brook, E. J., Martin, K., Chappellaz, J., Aoki, S., Nakazawa,

T., Sowers, T. A., Alley, R. B., Ahn, J., Sigl, M., Severi, M., Dunbar, N. W., Svensson, A., Fegyveresi, J. M., He, C., Liu, Z., Zhu, J., Otto-Bliesner, B. L., Lipenkov, V. Y., Kageyama, M., and Schwander, J.: Antarctic surface temperature and elevation during the Last Glacial Maximum, Science, 372, 1097–1101, https://doi.org/10.1126/science.abd2897, 2021.

Courville, Z. R., Albert, M. R., Fahnestock, M. A., Cathles IV, L. M., and Shuman, C. A.: Impacts of an accumulation hiatus on the physical properties of firn at a low-accumulation polar site, J. Geophys. Res. Earth Surf., 112, https://doi.org/10.1029/2005JF000429, 2007.

Eicher, O., Baumgartner, M., Schilt, A., Schmitt, J., Schwander, J., Stocker, T. F., and Fischer, H.: Climatic and insolation control on the high-resolution total air content in the NGRIP ice core, Clim. Past, 12, 1979, 2016.

Epifanio, J. A., South Pole ice core (SPC14) total air content (TAC), U.S. Antarctic Program (USAP) Data Center. doi: https://doi.org/10.15784/601546, 2022.

Epifanio, J. A., Brook, E. J., Buizert, C., Edwards, J. S., Sowers, T. A., Kahle, E. C., Severinghaus, J. P., Steig, E. J., Winski, D. A., Osterberg, E. C., Fudge, T. J., Aydin, M., Hood, E., Kalk, M., Kreutz, K. J., Ferris, D. G., and Kennedy, J. A.: The SP19 chronology for the South Pole Ice Core – Part 2: gas chronology, Δage, and smoothing of atmospheric records, Clim. Past, 16, 2431–2444, https://doi.org/10.5194/cp-16-2431-2020, 2020.

Fegyveresi, J. M., Alley, R. B., Spencer, M. K., Fitzpatrick, J. J., Steig, E. J., White, J. W. C., McConnell, J. R., and Taylor, K. C.: Late-Holocene climate evolution at the WAIS Divide site, West Antarctica: bubble number-density estimates, J. Glaciol., 57, 629–638, https://doi.org/10.3189/002214311797409677, 2011.

Fegyveresi, John M. Physical properties of the West Antarctic Ice Sheet (WAIS) Divide deep core: Development, evolution, and interpretation. The Pennsylvania State University, UMI: 37155012015, 2015.

Fegyveresi, J.M., Alley, R.B., Fitzpatrick, J.J., Voigt, D., Courville, Z. and Lieblappen, R., 2018, December. Measurement and interpretation of bubble number-density evolution through the upper 1200 meters of the SPC14 South Pole Ice Core (SPICEcore). In: AGU Fall Meeting Abstracts, December 2018, Washington D.C., C41C-1750, 2018AGUFM.C41C1750F, 2018.

1025 Fitzpatrick, J. J., Voigt, D. E., Fegyveresi, J. M., Stevens, N. T., Spencer, M. K., Cole-Dai, J., Alley, R. B., Jardine, G. E., Cravens, E. D., Wilen, L. A., Fudge, T. J., and Mcconnell, J. R.: Physical properties of the WAIS Divide ice core, J. Glaciol., 60, 1181–1198, https://doi.org/10.3189/2014JoG14J100, 2014.

Fudge, T. J., Lilien, D. A., Koutnik, M., Conway, H., Stevens, C. M., Waddington, E. D., Steig, E. J., Schauer, A.
1030 J., and Holschuh, N.: Advection and non-climate impacts on the South Pole Ice Core, Clim. Past, 16, 819–832, https://doi.org/10.5194/cp-16-819-2020, 2020.

Golledge, N. R., Levy, R. H., McKay, R. M., Fogwill, C. J., White, D. A., Graham, A. G. C., Smith, J. A., Hillenbrand, C.-D., Licht, K. J., Denton, G. H., Ackert, R. P., Maas, S. M., and Hall, B. L.: Glaciology and
1035 geological signature of the Last Glacial Maximum Antarctic ice sheet, Quat. Sci. Rev., 78, 225–247, https://doi.org/10.1016/j.quascirev.2013.08.011, 2013.

Goodwin, I. D., Browning, S., Lorrey, A. M., Mayewski, P. A., Phipps, S. J., Bertler, N. A. N., Edwards, R. P., Cohen, T. J., van Ommen, T., Curran, M., Barr, C., and Stager, J. C.: A reconstruction of extratropical Indo-
1040 Pacific sea-level pressure patterns during the Medieval Climate Anomaly, Clim. Dyn., 43, 1197–1219, https://doi.org/10.1007/s00382-013-1899-1, 2014.

Gregorich, M., Strohmaier, S., Dunkler, D., and Heinze, G.: Regression with Highly Correlated Predictors: Variable Omission Is Not the Solution, Int. J. Environ. Res. Public. Health, 18, 4259,
1045 https://doi.org/10.3390/ijerph18084259, 2021.

Gregory, S. A., Albert, M. R., and Baker, I.: Impact of physical properties and accumulation rate on pore close-off in layered firn, The Cryosphere, 8, 91–105, 2014.

1050 Huybers, P.: Early Pleistocene glacial cycles and the integrated summer insolation forcing, Science, 313, 508–511, 2006.

Kahle, E. C., Steig, E. J., Jones, T. R., Fudge, T., Koutnik, M. R., Morris, V. A., Vaughn, B. H., Schauer, A. J., Stevens, C. M., Conway, H., and others: Reconstruction of temperature, accumulation rate, and layer thinning

1055   from an ice core at South Pole, using a statistical inverse method, J. Geophys. Res. Atmospheres, 126, e2020JD033300, 2021.

Krinner, G., Raynaud, D., Doutriaux, C., and Dang, H.: Simulations of the Last Glacial Maximum ice sheet surface climate: Implications for the interpretation of ice core air content, J. Geophys. Res.-Atmospheres, 105, 2059–
1060   2070, https://doi.org/10.1029/1999jd900399, 2000.

Lee, J. E., Brook, E. J., Bertler, N. A. N., Buizert, C., Baisden, T., Blunier, T., Ciobanu, V. G., Conway, H., Dahl-Jensen, D., Fudge, T. J., Hindmarsh, R., Keller, E. D., Parrenin, F., Severinghaus, J. P., Vallelonga, P., Waddington, E. D., and Winstrup, M.: An 83\,000-year-old ice core from Roosevelt Island, Ross Sea, Antarctica,
1065   Clim. Past, 16, 1691–1713, https://doi.org/10.5194/cp-16-1691-2020, 2020.

Lilien, D. A., Fudge, T. J., Koutnik, M. R., Conway, H., Osterberg, E. C., Ferris, D. G., Waddington, E. D., and Stevens, C. M.: Holocene Ice-Flow Speedup in the Vicinity of the South Pole, Geophys. Res. Lett., 45, 6557–6565, https://doi.org/10.1029/2018GL078253, 2018.
1070

Lipenkov, V. Y., Raynaud, D., Loutre, M. F., and Duval, P.: On the potential of coupling air content and O-2/N-2 from trapped air for establishing an ice core chronology tuned on local insolation, Quat. Sci. Rev., 30, 3280–3289, https://doi.org/10.1016/j.quascirev.2011.07.013, 2011.

1075   Martinerie, P., Lipenkov, V. Y., and Raynaud, D.: Correction of Air-Content Measurements in Polar Ice for the Effect of Cut Bubbles at the Surface of the Sample, J. Glaciol., 5, 1990.

Martinerie, P., Raynaud, D., Etheridge, D. M., Barnola, J.-M., and Mazaudier, D.: Physical and climatic parameters which influence the air content in polar ice, Earth Planet. Sci. Lett., 112, 1–13, 1992.
1080

Martinerie, P., Lipenkov, V. Y., Raynaud, D., Chappellaz, J., Barkov, N. I., and Lorius, C.: Air content paleo record in the Vostok ice core (Antarctica): A mixed record of climatic and glaciological parameters, J. Geophys. Res. Atmospheres, 99, 10565–10576, 1994.

Mischler, J. A., Sowers, T. A., Alley, R. B., Battle, M., McConnell, J. R., Mitchell, L., Popp, T., Sofen, E., and Spencer, M. K.: Carbon and hydrogen isotopic composition of methane over the last 1000 years, Glob. Biogeochem. Cycles, 23, https://doi.org/10.1029/2009GB003460, 2009.

Mitchell, L. E., Brook, E. J., Sowers, T., McConnell, J. R., and Taylor, K.: Multidecadal variability of atmospheric methane, 1000–1800 CE, J. Geophys. Res. Biogeosciences, 116, 2011.

Mitchell, L. E., Buizert, C., Brook, E. J., Breton, D. J., Fegyveresi, J., Baggenstos, D., Orsi, A., Severinghaus, J., Alley, R. B., Albert, M., Rhodes, R. H., McConnell, J. R., Sigl, M., Maselli, O., Gregory, S., and Ahn, J.: Observing and modeling the influence of layering on bubble trapping in polar firn, J. Geophys. Res. Atmospheres, 120, 2558–2574, https://doi.org/10.1002/2014jd022766, 2015.

Morgan, J. D., Buizert, C., Fudge, T. J., Kawamura, K., Severinghaus, J. P., and Trudinger, C. M.: Gas isotope thermometry in the South Pole and Dome Fuji ice cores provides evidence for seasonal rectification of ice core gas records, The Cryosphere, 16, 2947–2966, https://doi.org/10.5194/tc-16-2947-2022, 2022.

NOAA, US Department of Commerce, Global Monitoring Laboratory - Data Visualization. url: https://gml.noaa.gov/dv/, (date accessed: Nov 19, 2021.)

Parrenin, F., Jouzel, J., Kawamura, K., Lemieux-Dudon, B., Loulergue, L., Masson-Delmotte, V., Narcisi, B., Raisbeck, G., Raynaud, D., Ruth, U., Schwander, J., Severi, M., Spahni, R., Steffensen, J. P., Svensson, A., Udisti, R., Waelbroeck, C., and Wolff, E.: The EDC3 chronology for the EPICA Dome C ice core, Clim Past, 13, 2007.

Raphael, M. N., Marshall, G. J., Turner, J., Fogt, R. L., Schneider, D., Dixon, D. A., Hosking, J. S., Jones, J. M., and Hobbs, W. R.: The Amundsen Sea Low: Variability, Change, and Impact on Antarctic Climate, Bull. Am. Meteorol. Soc., 97, 111–121, https://doi.org/10.1175/BAMS-D-14-00018.1, 2016.

Raynaud, D. and Lebel, B.: Total gas content and surface elevation of polar ice sheets, Nature, 281, 289, https://doi.org/10.1038/281289a0, 1979.

Raynaud, D. and Lorius, C.: Climatic Implications of Total Gas Content in Ice at Camp Century, Nature, 243, 283, https://doi.org/10.1038/243283a0, 1973.

Raynaud, D., Chappellaz, J., Ritz, C., and Martinerie, P.: Air content along the Greenland Ice Core Project core: A record of surface climatic parameters and elevation in central Greenland, J. Geophys. Res. Oceans, 102, 26607–26613, 1997.

Raynaud, D., Lipenkov, V., Lemieux-Dudon, B., Duval, P., Loutre, M.-F., and Lhomme, N.: The local insolation signature of air content in Antarctic ice. A new step toward an absolute dating of ice records, Earth Planet. Sci. Lett., 261, 337–349, https://doi.org/10.1016/j.epsl.2007.06.025, 2007.

Saltykov, S. A.: Stereometričeskaâ metallografiâ:(stereologiâ metalličeskih materialov), Metallurgiâ, 1976.
Schneider, D. P., Okumura, Y., and Deser, C.: Observed Antarctic Interannual Climate Variability and Tropical Linkages, J. Clim., 25, 4048–4066, https://doi.org/10.1175/JCLI-D-11-00273.1, 2012.

Schwander, J.: The transformation of snow to ice and the occlusion of gases, Environ. Rec. Glaciers Ice Sheets, 53–67, 1989.

Severinghaus, J. P., Sowers, T., Brook, E. J., Alley, R. B., and Bender, M. L.: Timing of abrupt climate change at the end of the Younger Dryas interval from thermally fractionated gases in polar ice, Nature, 391, 141–146, 1998.

Sowers, T., Bender, M., Raynaud, D., and Korotkevich, Y. S.: $\delta15N$ of N_2 in air trapped in polar ice: A tracer of gas transport in the firn and a possible constraint on ice age-gas age differences, J. Geophys. Res. Atmospheres, 97, 15683–15697, https://doi.org/10.1029/92JD01297, 1992.

WAIS Divide Project Members, Fudge, T. J., Steig, E. J., Markle, B. R., Schoenemann, S. W., Ding, Q., Taylor, K. C., McConnell, J. R., Brook, E. J., Sowers, T., White, J. W. C., Alley, R. B., Cheng, H., Clow, G. D., Cole-Dai, J., Conway, H., Cuffey, K. M., Edwards, J. S., Lawrence Edwards, R., Edwards, R., Fegyveresi, J. M., Ferris, D., Fitzpatrick, J. J., Johnson, J., Hargreaves, G., Lee, J. E., Maselli, O. J., Mason, W., McGwire, K. C., Mitchell, L. E., Mortensen, N., Neff, P., Orsi, A. J., Popp, T. J., Schauer, A. J., Severinghaus, J. P., Sigl, M., Spencer, M.

K., Vaughn, B. H., Voigt, D. E., Waddington, E. D., Wang, X., and Wong, G. J.: Onset of deglacial warming in West Antarctica driven by local orbital forcing, Nature, 500, 440–444, https://doi.org/10.1038/nature12376, 2013.

Winski, D. A., Fudge, T. J., Ferris, D. G., Osterberg, E. C., Fegyveresi, J. M., Cole-Dai, J., Thundercloud, Z., Cox, T. S., Kreutz, K. J., Ortman, N., Buizert, C., Epifanio, J., Brook, E. J., Beaudette, R., Severinghaus, J., Sowers, T., Steig, E. J., Kahle, E. C., Jones, T. R., Morris, V., Aydin, M., Nicewonger, M. R., Casey, K. A., Alley, R. B., Waddington, E. D., Iverson, N. A., Dunbar, N. W., Bay, R. C., Souney, J. M., Sigl, M., and McConnell, J. R.: The SP19 chronology for the South Pole Ice Core – Part 1: volcanic matching and annual layer counting, Clim. Past, 15, 1793–1808, https://doi.org/10.5194/cp-15-1793-2019, 2019.

Page 15: [1] Deleted   **Epifanio, Jenna**   **9/20/23 9:43:00 AM**

Page 29: [2] Deleted   **Epifanio, Jenna**   **9/20/23 11:02:00 AM**

Page 29: [3] Deleted   **Epifanio, Jenna**   **9/20/23 11:04:00 AM**

Page 35: [4] Deleted   **Epifanio, Jenna**   **9/20/23 11:05:00 AM**